Journal of Applied Physics

RESEARCH ARTICLE | FEBRUARY 23 2026

Impact of reverse flow induced by a sawtooth anode on the performance of an argon Hall thruster

Dibyesh Satpathy ; Kimiya Komurasaki ; Jiwon Lee ; Hokuto Sekine ; Nadine Barth ; Hiroyuki Koizumi

J. Appl. Phys. 139, 083303 (2026)
https://doi.org/10.1063/5.0307266

AIP Publishing

Journal of Applied Physics
ARTICLE
pubs.aip.org/aip/jap

Impact of reverse flow induced by a sawtooth anode on the performance of an argon Hall thruster

Cite as: J. Appl. Phys. **139**, 083303 (2026); doi: 10.1063/5.0307266
Submitted: 15 October 2025 · Accepted: 30 January 2026 ·
Published Online: 23 February 2026

View Online Export Citation CrossMark

Dibyesh Satpathy,[1,a)] Kimiya Komurasaki,[1] Jiwon Lee,[1] Hokuto Sekine,[1,2] Nadine Barth,[1] and Hiroyuki Koizumi[3]

AFFILIATIONS

[1]Department of Aeronautics and Astronautics, The University of Tokyo, Tokyo 113-8656, Japan
[2]Princeton Plasma Physics Laboratory, Princeton, New Jersey 08543-0451, USA
[3]Department of Advanced Energy, The University of Tokyo, Chiba 277-0082, Japan

[a)]**Author to whom correspondence should be addressed:** dibyeshsatpathy@g.ecc.u-tokyo.ac.jp

ABSTRACT

This study reports the performance comparison of the RAIJIN-66 TAL-type Hall thruster with argon propellant, using two hollow anode designs, one with a simple straight shape and another one with a sawtooth shape. Simulations of the rarefied gas in the sawtooth hollow anode region suggest a successful reversal of the direction of neutral particle flow, with an average increase in the neutral particle density by 15.5% when compared to the straight-shaped hollow anode. This contributes to the improvement in performance across a range of discharge voltages that was measured experimentally. When the thruster is operated with a discharge voltage of 150 V and a flow rate of 70 SCCM, the propellant utilization efficiency with the straight anode is 14%, while with the sawtooth anode it is 25.1%. The anode efficiency reaches in the vicinity of 15% with the sawtooth anode in high voltage conditions, exceeding the efficiencies achieved with the straight anode in the same operating conditions. The optimal magnetic field condition for argon operation and the tuning parameters of the sawtooth anode design for RAIJIN-66 are also discussed.

I. INTRODUCTION

The adoption of Hall thrusters for space applications has increased in significance. The demand for reliable yet affordable propulsion systems for space applications has increased markedly in recent years. As a result, electric propulsion systems, particularly Hall thrusters, have been extensively tested. Hall thrusters basically have two variants: Thrusters with Anode Layer (TAL) and Stationary Plasma Thrusters (SPT).[1] The propellant gas is introduced through a hollow anode in TAL, characterized by a shorter acceleration region surrounded by metal guard rings and biased at the cathode potential. In contrast, in the SPT, the propellant gas is similarly introduced through the anode but typically features a ceramic wall. In recent research, walls made of graphite have also been considered.[2,3] These walls encase the typically longer acceleration region instead of metal guard rings as in TAL. Although SPT and TAL differ in a number of important ways, TAL offers a higher thrust density than SPT typically in the low to moderate power range, although the difference mitigates when transitioning to high power operation.[4–6] Due to its lower ionization potential and higher atomic mass, xenon as a propellant in an electric propulsion system provides higher thruster performance. However, in recent years, the cost of xenon has been increasing exorbitantly, and a switch toward alternative propellants has become necessary. Among the propellants that have lower ionization energy and high atomic mass, the candidates include iodine and bismuth.[7,8] These two elements have been the subject of extensive research. Although for certain operating conditions they can outperform xenon-fed Hall thrusters, unfortunately, they also have severe drawbacks that are relatively difficult to manage. Iodine is chemically reactive and harmful to humans in larger doses and also reacts with chamber walls, requiring special chambers for testing, increasing the cost of research and development.[9] Bismuth is radioactive and requires stringent high thermal control due to its high boiling point.[10] Metal propellants like zinc and magnesium offer some advantages over xenon, for example, low ionization energy and high storage density. However, like bismuth, the temperature control system is extremely complicated, which limits its applicability.[11] Krypton and argon are two relatively easy-to-access propellants, with the cost of argon per liter being 1000 times cheaper than that of krypton. SpaceX recently demonstrated krypton and argon Hall thruster operation in their Starlink satellites. Compared to xenon and krypton, argon is not only inefficient due to its higher ionization potential and significantly lower atomic mass but also requires larger tanks for propellant storage due to its lighter density.[12,13] As such, it is essential to achieve high efficiencies with a low mass flow rate to also reduce the tank size requirements.

Although the physical parameters of a propellant that affect performance are constant, a variable parameter is the available neutral particle density. This parameter is affected by the anode mass flow rate, the local cross-sectional area of the region of interest, and also the local neutral particle velocity. Although the mass flow rate is variable based on goals, for controlled comparisons the mass flow rate will remain the same throughout the operation to avoid changes in discharge current. The cross-sectional area also remains fixed for a given thruster design; the only variable parameter ultimately is the neutral particle velocity, and this should therefore be optimized because lighter propellants like argon will have higher thermal velocity due to their lower atomic mass. The thermal velocity of the neutral atom can be altered by ideally controlling the anode temperature, as described by the authors in their previous work.[14] We reported that as the anode temperature increased from 320 to 480 K, the propellant utilization efficiency during argon operation at an anode flow rate of 60 SCCM and a discharge voltage of 230 V, reduced from 39% to 24% as measured experimentally. Theoretically, it was estimated that when the anode temperature reaches 800 K, the propellant utilization efficiency reaches 12%, making it impractical. The authors have also reported a similar association between anode temperature increase and performance decay using xenon propellant,[15] and other researchers have evaluated such associations using comparisons of cooled and uncooled anodes and by removing the primary heating mechanism of the anode.[16–18] Fundamentally, when the anode temperature increases, the neutral particle velocity increases and these particles escape the ionization region without ionization, resulting in a decrease in the effective available neutral particle density, which deteriorates the propellant utilization efficiency and, eventually, the thruster performance.[19] Passive cooling methodologies, for example, cooling through radiators or oscillating heat pipes, can be considered practical approaches toward cooling;[20,21] however, their efficacy is limited, specifically when concerning with the efficiency of alternative propellants. Although active anode cooling is an attractive measure for enhancing the performance of argon-fed Hall thrusters, it is challenging to implement in small-to even moderate-scale satellites because active cooling using fluid would require a pump to circulate around the anode, which would consume a large fraction of the available satellite mass.[22]

To counteract the high thermal velocity, the typical axial injection of the propellant can be altered. The authors previously evaluated the comparison of the axial and swirl injection method and reported an increase in performance in the low to moderate voltage case, with an increase in measured thrust of 12.5%, 6.9%, and 2% with discharge voltages of 150, 200, and 250 V, respectively.[23] Using the swirl injector, the neutral particle density increased by 7.8% in the ionization region. One key aspect observed by the authors was that although the swirl injection method significantly increased the neutral particle density in the vicinity of the injection point (more than 30%), due to wall-induced losses, the increase in the neutral particle density in the ionization region was lower than expected. However, this can be addressed by incorporating a shorter anode length (relative to the anode width) into thrusters.[24] Nevertheless, the anode wall design marks a significant step in controlling the neutral particle velocity in Hall thrusters. Similar studies on alternate injection schemes using experimental and numerical methods have been reported by other researchers using radial injection,[25] circumferential injection,[26,27] reverse injection,[28] combined axial and alternative injection,[29,30] and changing injection location.[31,32] All these methods report improvement in neutral particle density, which aided in performance enhancement.

Ding *et al.*[33] developed an indented wall and this successfully improved the performance of xenon-fed Hall thrusters operating under low flow rate conditions. With the indented anode, the propellant utilization efficiency was greater than that of the straight anode at the same operating point, and the maximum difference was 8.35% when the discharge voltage was 400 V and the anode mass flow rate was 1.1 mg/s. A similar design approach was used in a micro-Hall thruster by Lu *et al.*[34] and reported similar improvements in thruster performance. Xu *et al.*[35] developed an Azimuthal Diversion Rail (ADR) to reduce the neutral particle velocity to increase the residence time of atoms in the discharge channel. Under low flow rate conditions of 1.5 mg/s, the propellant utilization efficiency was reported to be 57% with straight anode while with ADR the efficiency was 64%. With an increasing flow rate, the performance gap between the two cases was reduced and fully saturated to 91% at a flow rate of 5 mg/s. Ding *et al.*[36] also investigated the influence of inward oblique channel exit, which changed the neutral particle density, and led to a more global performance improvement due to an increase in the ionization rate and a decrease in the ion bombardment into the wall. Yamamoto *et al.*[37] adjusted the diameter of the far end of the discharge channel, resulting in three configurations: divergent, convergent, and parallel. According to their results, the divergent type has the opposite effect on local plasma viscosity and oscillation amplitude at low magnetic field strengths. Furthermore, because of a local increase in the neutral particle density, the convergent type efficiently boosts propellant utilization. It is important to note that the choice of the design of such anode walls or channel walls is determined by the reflective behavior of neutral gas, which is dependent on the species of propellant, the wall material, and finishing of the wall surface at the microscale level.[38,39]

This study reports on the performance comparison of a hollow anode with a sawtooth-walled shape and a simple straight wall shape, in a Thruster with Anode Layer, known as RAIJIN-66,[40] with argon as a propellant. Because of the lower mass of the argon propellant, the performance decay with anode temperature is severe, and, as such, a novel anode design becomes an essential step for achieving a lower neutral particle velocity for performance enhancement. This paper is divided into five sections, including this section regarding the introduction. In Sec. II, we describe the design details of the sawtooth anode and discuss the experimental setup and the numerical approach used in this study for the evaluation of performance and neutral gas dynamics. In Sec. III, the numerical and experimental results of this study are reported, which is followed by a discussion of our results in Sec. IV. Finally, we conclude our findings in Sec. V.

II. EXPERIMENTAL SETUP AND NUMERICAL MODELING

A. Hollow anode of RAIJIN-66

Figure 1(a) shows the photograph of RAIJIN-66 with the cross section of RAIJIN-66 in its original configuration shown in Fig. 1(b). RAIJIN-66 is a 66 mm outer diameter TAL type Hall thruster, with its anode made of copper and has a short channel (guard rings) of 2.1 mm in length. This thruster was originally developed for 2 kW xenon operation in a magnetically shielded configuration using trim yoke parts. For stable argon operation, the trim yoke parts were removed, and this study is conducted in an unshielded case. For the evaluation of this study, two anode designs with the same exit cross-sectional area were made, one with a simple straight anode wall and one with a sawtooth-shaped wall, as shown in Figs. 1(c) and 1(d). The purpose of using the sawtooth anode is to reverse the direction of the default axial flow of the propellant. The straight anode wall was designed to mitigate any possible influence on the axial flow as was possible with the previous default anode of the RAIJIN-66; to ensure a fair comparison. The design details of the sawtooth anode are shown in Fig. 2(a). The sawtooth anode has seven slits cut into the anode. The distance between each slit is 2.4 mm; this value ensured a good fit between the swirl injector and the upstream end of the slit. The sawtooth angle was kept at 60° as shown in Fig. 2(a) (the choice of angle selection is described in Sec. III A). The photographs of the sawtooth anode are shown in Figs. 2(b) and 2(c).

The heat load on the anode is dominantly governed by the product of the electron temperature and the discharge current.[41] In the presence of a pointed sawtooth structure, there can be a chance of melting the tips of the anode. As such, R0.3 fillet is included to mitigate the chances of tip melting. The fillet limits the possible electron concentration, which can otherwise influence the plasma, and it also reduces the probability of arcing, which can otherwise affect the operation stability. These two anode designs are coupled with the swirl injector used in the previous study, which was found to enhance thruster performance compared to the default axial injector.[23] With the swirl injector, the propellant is injected tangentially relative to the inner anode at acoustic velocity, significantly reducing the axial diffusion velocity. Table I shows the physical parameters of the injectors used in RAIIJIN-66.

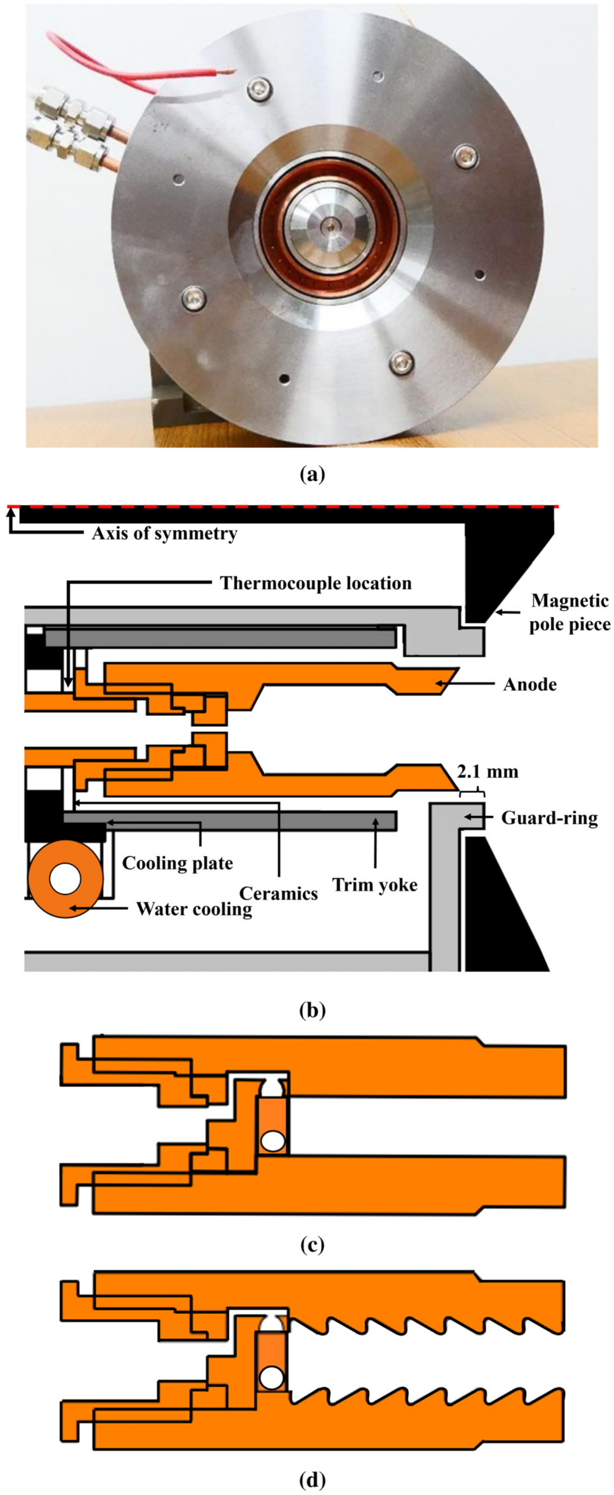

FIG. 1. Photograph of RAIJIN-66 (a), cross section of RAIJIN-66 in original configuration (b), straight anode (c), and sawtooth anode (d) used in this study.

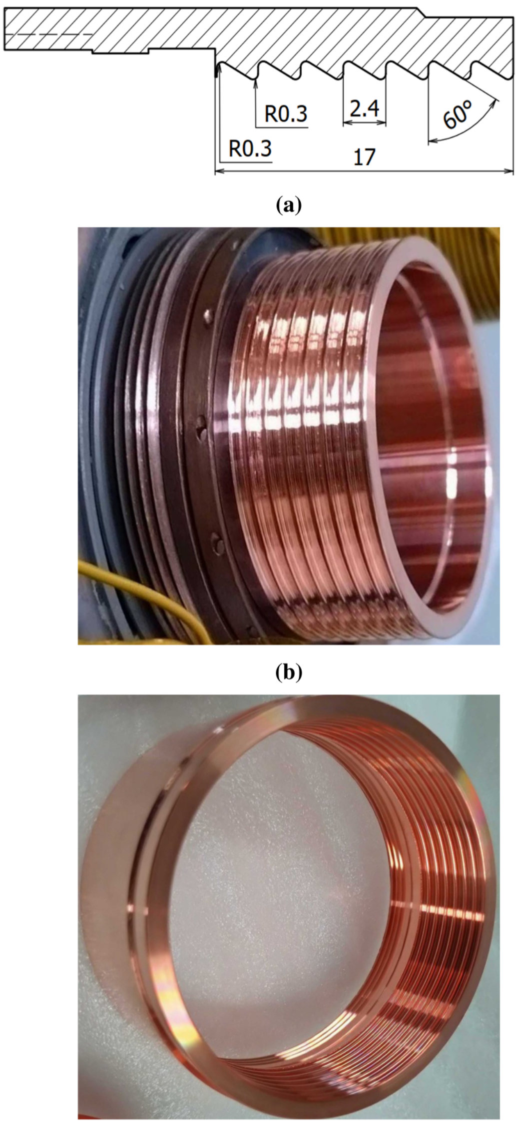

FIG. 2. Design details of sawtooth anode (a). Photographs of sawtooth inner anode (b) and sawtooth outer anode (c).

B. Experimental setup

All experiments were conducted in a stainless-steel cylindrical vacuum chamber of 2 m in diameter by 3 m in length using 99.99% argon, evacuated using a diffusion pump (PFL-36, ULVAC) with a pumping speed of 37 000 l/s, backed by two rotary pumps (PKS-070, ULVAC) with a pumping speed of 250 l/s each and one mechanical booster pump (PMB-060B, ULVAC) with a pumping speed of $2778 \times \mathrm{l/s}$. The chamber pressure was measured using a GL-D7 ionization gauge. Subsequently, the gas flow was controlled

TABLE I. Characteristics of a RAIJIN-66 propellant injector.

	Axial injector	Swirl injector
No. of orifices	24	14
Diameter of orifice	1 mm	1.5 mm
Injector angle relative to radius	…	60°
Orifice length	1.8 mm	2 mm
Injection velocity	Mach 1 (axial direction)	Mach 1 (tangential direction)

using two mass flow controllers (MODEL 3200, KOFLOC; Full Scale accuracy of 1%) for the thruster and one (MODEL 3660, KOFLOC, Full Scale accuracy of 1%–1.5%) for the cathode. The hollow cathode used in this study was manufactured by Plasma Controls, LLC, and 11 SCCM argon was supplied to the cathode during operation for all experiments.

Experiments were conducted with discharge voltages up to 300 V, under anode mass flow rate condition of 70 SCCM (5 Aeq/2.07 mg/s). The power supply GEN300-11-3P200-D from TDK-Lambda has been used in this study, which is capable of a rated output power of 3300 W. The pressure in the chamber during the experiment is 4×10^{-5} Torr, measured using an ionization gauge (ULVAC GI-D7) capable of measuring pressure in the range of 4×10^{-3} Torr to 9.75×10^{-9} Torr. RAIJIN-66 was designed for a discharge power of 2 kW with xenon propellant. However, inefficiencies associated with the thruster operation using argon significantly increase the heat load on the thruster, and to limit the heat load, the discharge power was lowered by reducing the mass flow rate during the operation. Although this affects performance, possible thermal damage to the thruster is eliminated. All experiments were conducted with a magnetic flux density of 45 mT (the method of selection is described in Sec. III B, where comparisons are made between magnetic flux density cases of 30, 45, and 60 mT). To ensure that the total flux of the particles remains the same for comparison, the performance is compared at a common anode base temperature across all the experiments. This anode temperature was measured by a K-type direct contact thermocouple, attached to the anode base, as shown in Fig. 1(b), but with a straight or sawtooth anode wall configuration. It should be noted in this study that the guard-ring is made of graphite, while in the previous study it was made of stainless steel. The new material was considered solely to extend the thruster lifetime.[42]

In this study, real-time measurements are relevant, where the performance is sensitive to the anode base temperature and, as such, all comparisons are made at a fixed anode base temperature of 350 K, which corresponds to the equilibrium anode base temperature in the case of 150 V operation with a straight anode. Although typically for ion beam current measurement a Faraday probe is used, the recommended practice is to sweep the probe downstream of the thruster under thermally steady-state conditions.[43] For real-time ion beam current measurement as required in this study, an ion collector plate was used. Assuming a symmetric ion beam, a quarter of the beam inside the divergence angle of about $\pm 45^\circ$ was collected by this plate. This plate was biased at a negative potential of 40 V to repel the incoming electrons.[44] The measured ion beam current was corrected using the copper SEE yield γ_{SEE} of 0.1094. The standard error in ion beam current measurement for the anode temperature of interest was evaluated based on standard deviation from multiple experiments that were conducted for reproducibility, and the error was found to be 2.5%. The propellant utilization efficiency is calculated from the measured ion current for singly charged ions in the plasma plume as

$$\eta_u = \frac{I_b m_i}{e \dot{m}_A}. \tag{1}$$

Here, I_b is the ion beam current, m_i is the mass of the ion, e is the elementary charge, and $\dot{m}_A$ is the anode mass flow rate.

In addition to ion beam current measurement, for real-time measurement of thrust T, a dual pendulum thrust stand, which is a null-type stand and permits thermal drift free real-time thrust measurement with a maximum signal drift of 3%.[45] The thrust signal was calibrated using a pulley and weight system.[15] Once the thrust is measured, the anode efficiency and the specific impulse are evaluated as

$$\eta_A = \frac{T^2}{2\dot{m}_A P_D}, \tag{2}$$

$$I_{SP} = \frac{T}{\dot{m}_A g}. \tag{3}$$

Here, P_D and g are the discharge power and the standard acceleration of gravity, respectively.

C. Numerical setup

To evaluate the neutral gas behavior inside the RAIJIN-66 annulus, the direct simulation Monte Carlo (DSMC) solver called dsmcFoam+, which is an OpenFoam open source package, is used.[46] As wall reflections dominate the flow behavior under rarefied flow conditions, the Cercignani-Lampis-Lord (CLL) reflection model is implemented.[47] Based on experiments of an argon atom reflecting off a copper plate,[38] the tangential and normal accommodation coefficients of 0.9 and 0.75, respectively, were chosen. Figure 3 shows the distribution of the polar probability density of an argon atom with an incident angle of 5° and 60°. The reflective behavior of an atom from a surface is governed dominantly by the accommodation coefficient, which is defined in gas–surface interaction as a quantifiable way of judging how strongly atom velocity components adjust to the wall during reflection. Considering the higher values of the tangential and normal accommodation coefficients of argon, the reflective behavior can be considered highly diffusive. The normal and tangential accommodation coefficients are different from the thermal accommodation coefficient, which has been assumed to be one for this study; having a value of one correlates to full accommodation to the anode temperature. Although temperature gradients can exist between the anode base and the anode tip and can vary between a straight anode and a sawtooth anode, these have not been incorporated in this study, and the

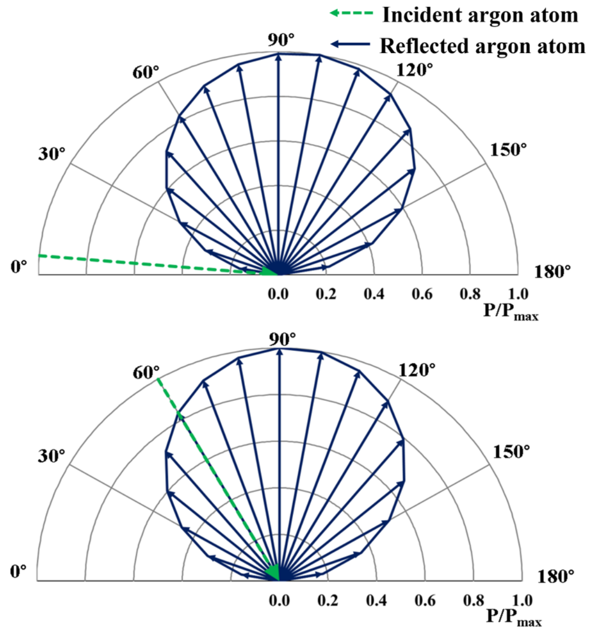

FIG. 3. Polar probability density distribution of reflected argon for the case with an incident argon atom angle of 5° and 60°, obtained by the CLL model that reproduces Sharipov's measurement.[38] Dashed line indicates the incoming argon atom, while the solid lines indicate the probable direction of argon atom after reflection.

comparisons between the two anodes were done with uniform anode temperatures of 350 and 500 K. Here, 350 K refers to the anode temperature condition for experimental comparison, which is the equilibrium anode base temperature for 150 V operation with a straight anode, and 500 K refers to the evaluation of the effectiveness of the sawtooth anode at higher anode temperatures when comparing to a straight anode with lower anode temperatures. It should be noted that in this simulation, all particles touching the patch at guard-ring exit (the boundary region corresponding to the end of the simulation domain) get deleted from the domain.[23] This implies a vacuum condition at this patch, and the neutral conditions downstream of the exit, for example, in the annular region corresponding to the pole piece, are not simulated. Table II shows the parameters and boundary conditions used in the DSMC simulations for this study.

III. RESULTS

A. Numerical results

1. Neutral gas dynamics in straight and sawtooth anode

With a straight anode, several particles escape the relevant ionization region quickly because they do not undergo sufficient reflections from the wall. Additionally, several particles can also reflect off the parallel shape anode and move downstream instead of upstream (backflow), and this further aids in the escape of

TABLE II. Parameters for DSMC simulation.

Boundary conditions	Value/characteristic
Injection condition	
Flow rate	70 SCCM
Velocity	Mach 1
Exit condition	Particle deletion upon contact with the outlet
Particle species name	Argon (Ar)
Reflection conditions	
Tangential acc. coefficient	0.9
Normal acc. coefficient	0.75
Wall temperature	350 K, 500 K
Simulation properties	
Time step	1×10^{-7} s
Particle ratio	1×10^{5}
Mesh size	1×10^{-4}
Inter-particle collision condition	Variable Hard Sphere model

neutral particles without ionization. Controlling neutral particles that simply escape the ionization region upon injection can be done by changing the injection direction, as has been attempted by the authors previously.[23] However, controlling the reflective behavior requires special designs of the anode wall such as the sawtooth anode, which restrict the reflected particles from moving downstream. Figure 4(a) shows the neutral particle density color contour map. The darker region is more pronounced upstream of the sawtooth anode than in the straight anode, which corresponds to significant backflow owing to the sawtooth anode. Figure 4(b) shows the spatially averaged neutral particle velocity distribution along the axial direction. Neutral particle velocity slows down near the inlet due to some backflow being caused by particles colliding with the wall and being emitted isotropically. These neutral particles have velocities in both directions toward the anode center, which tend to cancel each other out and limit the decline in the density of neutral particles. Toward the anode exit, there is no backflow because reflections create a dominant forward flow toward the exit, and this causes the neutral particle velocity to increase more rapidly. In the case of the straight anode, the axial distribution of velocity is as expected,[48] but in the case of the sawtooth anode, the particles reflect off the angle sections and enhance backflow, and the accelerating behavior of the particles is well controlled. The pattern of reduction of neutral particle velocity followed by an increase and then followed by a reduction again suggests that the flow directionality reverses.

Figure 5(a) shows the differences in the neutral particle density averaged in the cross section of the anode and channel, where L_c refers to the length of the channel or guard-ring and L_i refers to the ionization region length. The channel length is based on thruster geometry and ionization region length is influenced by the width of the magnetic flux density. The ionization region length was estimated in our previous study by curve-fitting the measured dependence of propellant utilization efficiency on anode temperature change. For RAIJIN-66 in unshielded condition, it has

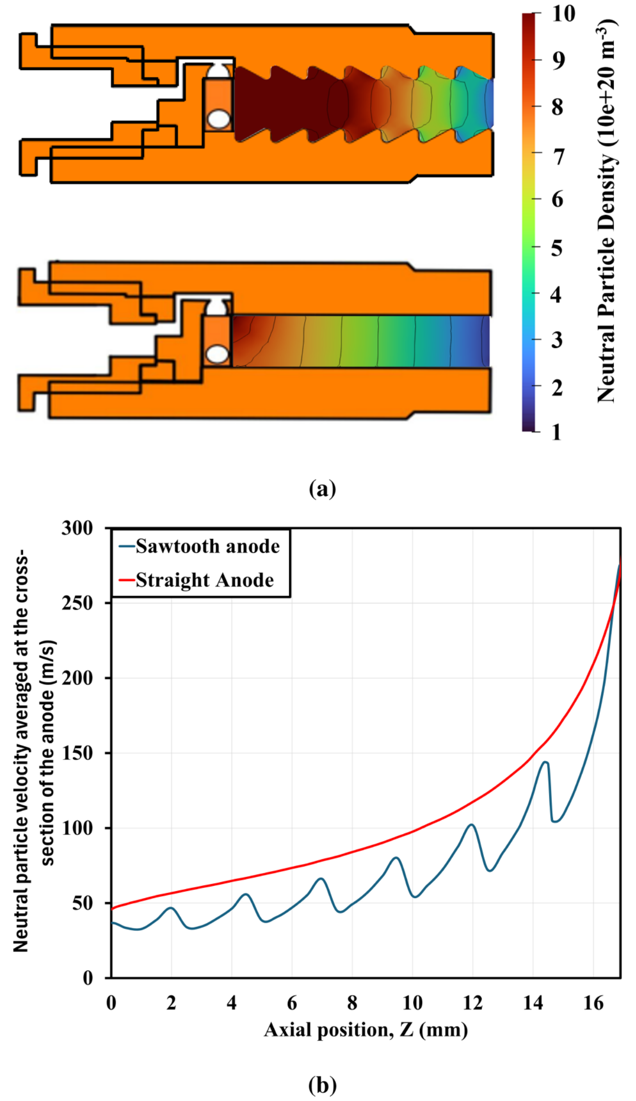

FIG. 4. Neutral density color contour map of two anodes (a) and axial distribution of neutral particle velocity from start of anode wall to anode exit (b).

an approximate value of 5.6 mm and is assumed to fully encompass the channel length.[14]

With the sawtooth anode, there are bumps in the neutral particle density distribution, which suggests that neutral particles indeed undergo successful reflections, which causes flow reversal. Taking into account the 350 K anode temperature case for both anode designs, due to the significant backflow of the seven sawtooth anode slits, the neutral particle density increases by 22.1% at $Z = 0$ (Z corresponds to the distance from the start of the hollow anode), although the injection conditions remain the same. At $Z = 8$ mm, the neutral particle density with the sawtooth anode is 23.8% higher compared to the straight anode. It is slightly higher

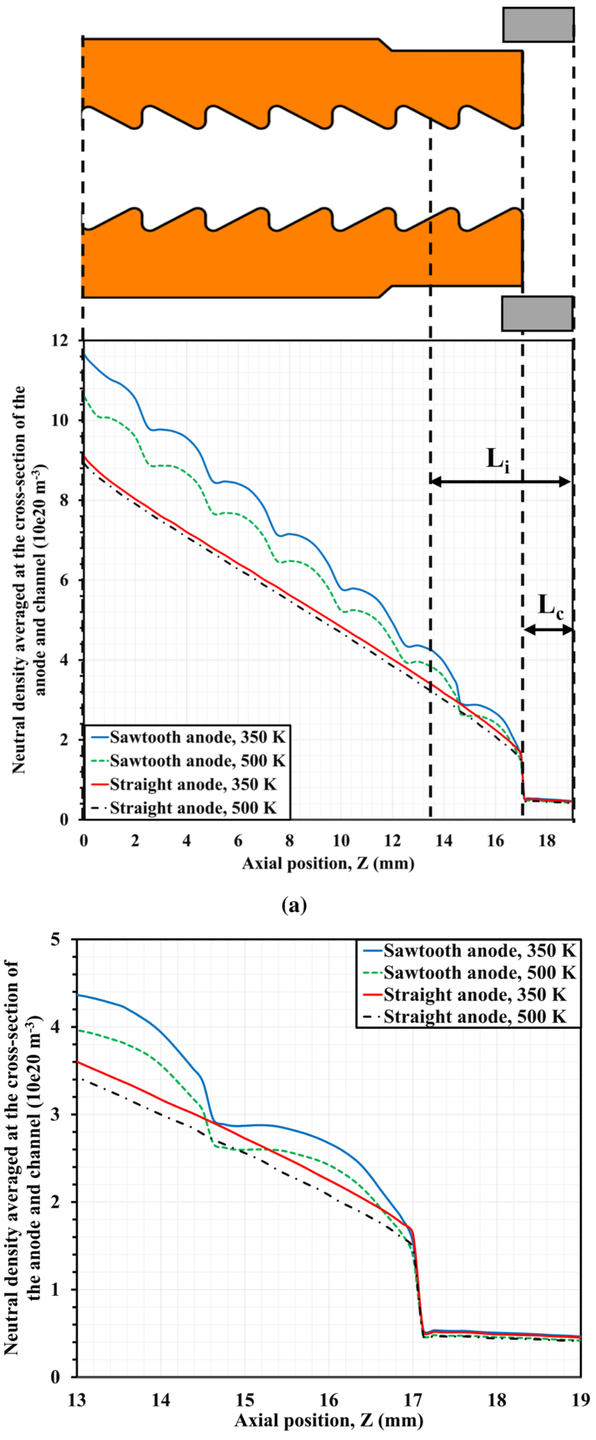

FIG. 5. Comparison of the straight and sawtooth anode neutral density averaged at the cross section, from the start of anode wall to channel exit (a), in the expected ionization region (b).

than the upstream condition, because the sawtooth anode design incorporates slanted structures promoting higher local density in between two successive slits. Considering the ionization region length of 5.6 mm as estimated in a previous study,[14] and assuming that the ionization region ends exactly at the exit of the guard-ring, the region of interest in this study is from $Z = 13.5$ to 19.1 mm (guard-ring exit). The maximum visible gain in neutral particle density in the ionization region is 20.3% and the minimum visible gain is 3.21% (specifically in the guard-ring region). The average gain in neutral particle density throughout the 5.6 mm length of the ionization region is 15.5%. The particles reflecting off the sawtooth anode in the ionization region have very low velocity, and consequently the probability of ionization becomes higher. Analogous to the neutral particle density, the difference in neutral particle velocity is 15.5%, with the sawtooth anode showing very low neutral particle velocity. The simulations with 500 K case for both anodes suggest a similar improvement in neutral particle density, although overall values for both the anodes are lower due to higher thermal velocity, compared to the lower temperature conditions. The average neutral particle density increases by 7.4%, when the result of the sawtooth anode with 500 K is compared to that of the straight anode with 350 K, as shown in Fig. 5(b).

2. Sawtooth anode design choice

To determine the angle of the sawtooth in RAIJIN-66, three designs of the sawtooth anode were investigated using the sawtooth angle as the tuning parameter. Since the available length of 17 mm from the injector to the anode exit is fixed for RAIJIN-66; as such, the only tuning parameter here was the angle. Although the depth of the slit cut in the anode can be deeper, structural integrity of the anode should be considered; as a result, this was kept the same as the original RAIJIN-66 anode design.[40] Additionally, in all three designs, the cross-sectional area at the exit of the anode was kept the same as shown in Fig. 6. As the angle is reduced, the number of slits that can be cut into the anode will increase. This changes from 7 for 60° to 15 for 30°; the pitch is lower between two consecutive slits as the angle is reduced. The comparison of the axial distribution of the neutral particle density averaged at the cross section of the anode and channel for the three considered angles is shown in Fig. 6. Compared to the 60° case, the improvement in the neutral particle density with 45° is 3.1% and the difference between the 45° case and the 30° case is 2.7%, as shown in Fig. 7(a). Relative to the straight anode, the 60°, 45°, and 30° cases have 15.5%, 18.6%, and 21.3% higher neutral particle density, respectively. Since the increment in neutral particle density is small with each successive design, the influence of pitch can be considered minimal. Additionally, because the manufacturing cost is sensitive to the number of slits, 60° was chosen in this study.

B. Experimental results

1. Choice of magnetic field

One key aspect of operating argon-fed Hall thrusters is the choice of magnetic flux density to ensure maximum efficiency. Anode layer thrusters operating with xenon operate efficiently with a high magnetic flux density, whereas those operating with argon

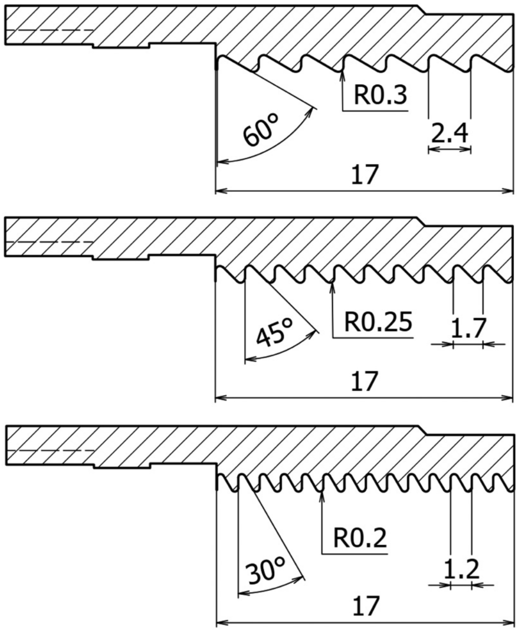

FIG. 6. Design of sawtooth anode with different angle.

achieve maximum efficiency with a low magnetic flux density. This has been attributed to the argon optimal operating regime being in classical diffusion and that of xenon being in the anomalous regime.[13] When the electron transport is governed by neutral atom and ion collisions, it can be considered in a classical diffusion regime. However, if the electron transport is governed by plasma turbulence and near-wall conductivity, then it can be considered an anomalous diffusion regime. The two modes can be distinguished based on diffusion coefficients for each case, which are proportional to the inverse of the square of magnetic flux density B for the classical regime and the inverse of B for the anomalous regime. Our previous work showed that classical cross-field mobility scales as

$$\mu \propto \frac{Q\sigma\sqrt{M_n}}{B^2}, \tag{4}$$

where Q is the neutral throughput, σ is the elastic collision cross section and M_n is the neutral atom mass. As electron velocity can be taken as the product of cross-field mobility and electric field, xenon, being heavier, tends to lose electrons easily compared to argon at the same conditions, unless B is increased. Once B is high, the transport is instability driven, which allows strong confinement while still supplying enough electron transport to sustain the discharge. The lower magnetic flux density in the classical diffusion region contributes to reduced oscillation amplitudes, which is crucial to maintain stable thruster operation.[13] To evaluate the appropriate value of magnetic flux density during argon operation, three experiments were conducted at a discharge voltage condition of 250 V with 70 SCCM of argon anode flow rate and with a magnetic flux density of 30, 45, and 60 mT as shown in Fig. 8 under steady-state operation. In the case of 30 mT, the equilibrium anode temperature reaches 500 K. As such, the propellant utilization efficiency is 34.1%. In the case of 45 and 60 mT, the equilibrium anode temperature is 460 and 465 K, respectively. The propellant utilization efficiencies are 37.7% and 37.1% for the 45 and 60 mT case, respectively.

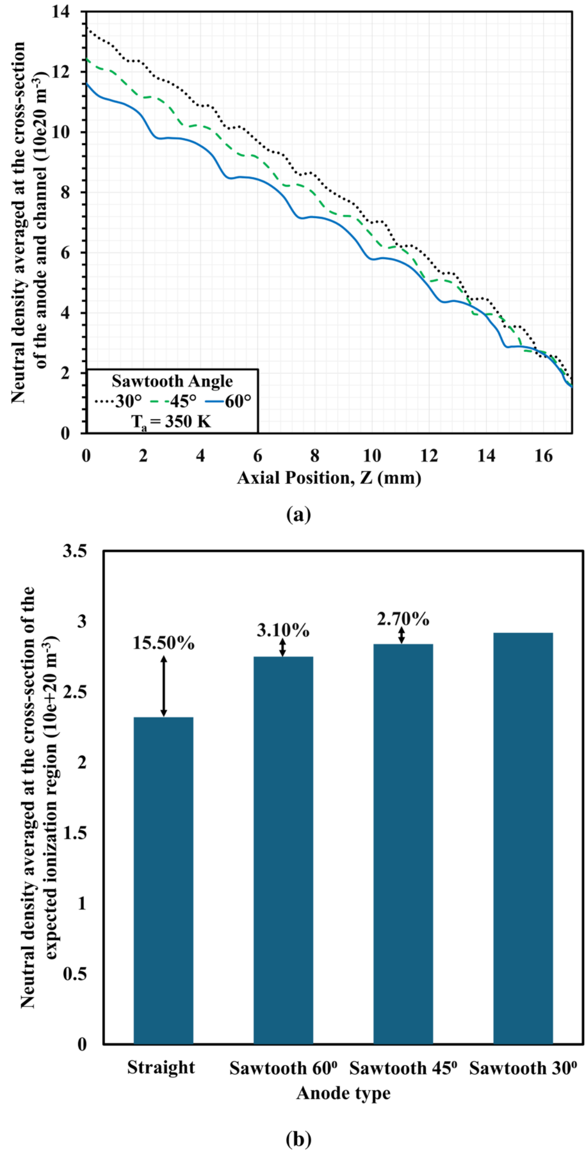

FIG. 7. Design of sawtooth anode with different angle (a) and influence of sawtooth angle (b).

Although the difference between the 45 and 60 mT cases is negligibly small, a higher coil current is necessary to operate the thruster with 60 mT. This causes an increase in the thermal load, and as such, the anode temperature is slightly higher in the 60 mT

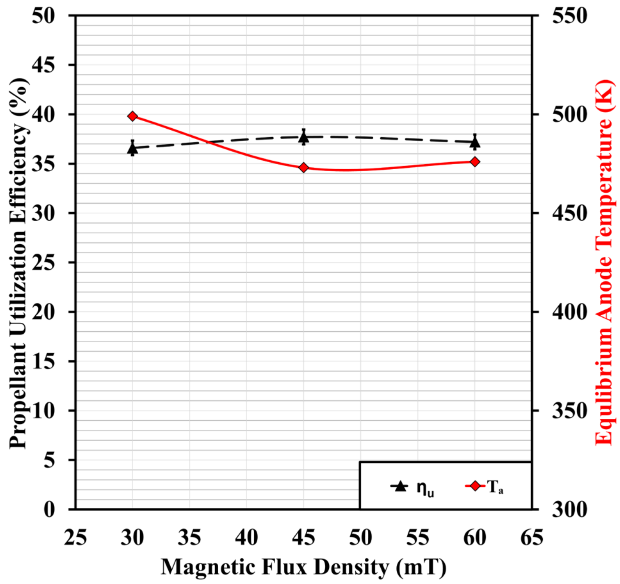

FIG. 8. Effect of magnetic flux density on propellant utilization efficiency.

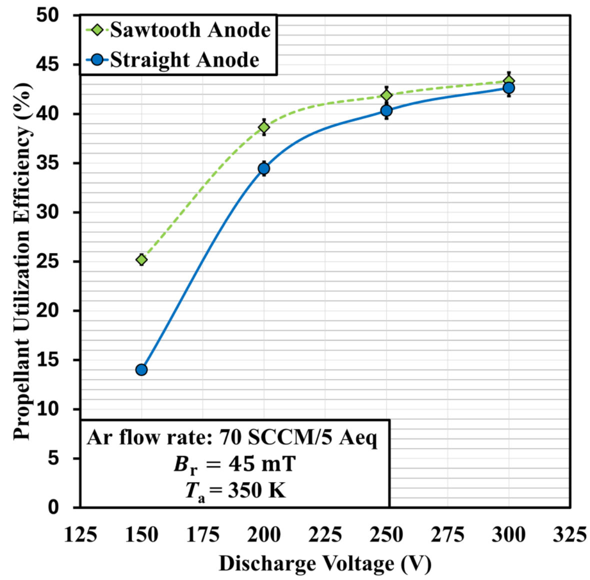

FIG. 9. Comparison of propellant utilization efficiency.

case. It is to be noted that this result can be influenced by increased beam collimation with high magnetic flux density,[49] which can cause some ions to be lost to the inner wall. Finally, 45 mT was chosen for all comparison experiments. This evaluation also shows the importance of anode temperature control for maximizing the performance of argon-fed Hall thrusters.

2. Performance comparison

Figure 9 shows the comparison of propellant utilization efficiency with the sawtooth and straight anode at an anode base temperature of 350 K, which was the equilibrium anode base temperature for the straight anode when operated with 150 V. When the discharge voltage is 150 V, the propellant utilization efficiency with the straight anode is 14%, while with the sawtooth anode it is 25.1%. With 200 V, the propellant utilization efficiency with the straight anode is 34.4% and with the sawtooth anode it is 38.7%. As the discharge voltage increases to 250 V, the propellant utilization efficiency gap between the two injectors is relatively small; that is, with the straight anode it is 40.3%, while with the sawtooth anode it is 41.9%, and with 300 V, the propellant utilization efficiency is nearly saturated, with the efficiency 42.7% and 43.2% with the straight and sawtooth anode, respectively.

The thrust performance measurements also suggest improvements in performance, as shown in Fig. 10(a), which shows that with 150 V, the thrust improves by 44% using the sawtooth anode. With 200 V, the thrust improvement is 12.4% and with 250 V the improvement is 5.6%, while with 300 V the gain is 1.8%. The improvement in thrust with the sawtooth anode can be considered to be predominantly influenced by the enhancement of propellant utilization efficiency; beam divergence also influences the thrust, and other studies have reported changes in beam divergence in a limited manner with anode or channel wall design.[31,35] The anode efficiency reaches a value greater than 15% and the thrust-to-power ratio improves, indicating improvement in ionization performance when using the sawtooth anode, as shown in Fig. 10(b).

IV. DISCUSSION

A. Influence of low neutral velocity

The neutral density in the ionization region can be given as[18]

$$n_{\mathrm{n}} = (1 - f_{\mathrm{i}})\frac{\dot{m}_{\mathrm{A}}}{M_{\mathrm{n}} A v_{\mathrm{n}}}, \tag{5}$$

where n_n is the neutral particle density, f_i is the fraction of neutral argon atoms that have been ionized in the ionization region, A and v_n are the cross-sectional area and neutral particle velocity in the relevant region, respectively. Considering the low velocity achieved by using a sawtooth anode, the neutral particle density in the ionization region will be higher and this will improve the ionization rate

$$\dot{n}_{\mathrm{i}} = n_{\mathrm{n}} n_{\mathrm{e}} \langle \sigma_{\mathrm{i}} v_{\mathrm{e}} \rangle. \tag{6}$$

Here, n_e represents the electron density and $\langle \sigma_i v_e \rangle$ is the ionization rate coefficient. This then enhances the ion beam current and ultimately the propellant utilization efficiency as ion beam current is directly proportional to the ionization rate[50]

$$I_{\mathrm{b}} = e\dot{n}_{\mathrm{i}}. \tag{7}$$

If the ionization region length can be extended upstream, a much larger fraction of neutral particles is likely to ionize, and the benefit

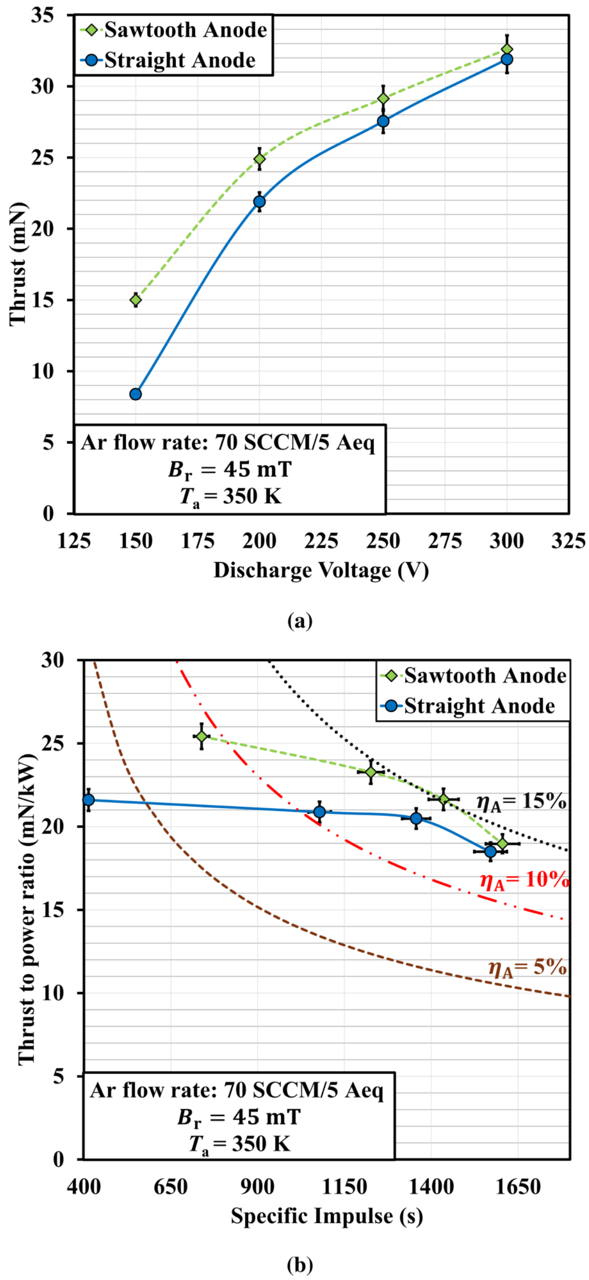

FIG. 10. Comparison of thrust (a) and thrust performance (b).

of the sawtooth anode design with several sawtooth slits can be considered to the maximum extent. The ionization region can be shifted upstream by redesigning the magnetic pole-piece parts of RAIJIN-66. The width of the magnetic flux density plays a dominant role in determining the length of the ionization region.[14,51,52] The location of ionization can also be influenced by the location of the peak position of magnetic flux density.[53] As such, the ionization region can be shifted upstream and enlarged by shifting the peak magnetic flux density position upstream with a wider axial distribution of the magnetic flux density toward the upstream. In the opposite condition, where the ionization region length is short, like in a magnetically shielded configuration, several slits will not have similar significance, and in such a case, fewer slits can be considered in the ionization region.

B. Performance trends

From the experimental results, it can be observed that the gain in propellant utilization efficiency, regardless of anode design choice, is large when the discharge voltage is increased from 150 to 200 V or from 200 to 250 V, but when the discharge voltage is increased from 250 to 300 V, the gain is small. This happens due to a combination of factors.

Poli *et al.*[54] evaluated that the volumetric ion production in the channel of a Hall thruster can be given as

$$S_i = n_n n_e \bar{v}_e \sigma_{\mathrm{i}} \left[1+\frac{T_e E_{ion}}{(T_c+E_{ion})^2}\right]\exp\left(\frac{-\mathrm{E_{ion}}}{\mathrm{T_e}}\right). \tag{8}$$

Here, $\bar{v}_e$ is the mean electron thermal velocity, σ_{i} is the ionization cross-section, E_{ion} is the ionization potential of propellant species, and T_{e} is the electron temperature. However, not all ions produced are exhausted downstream from the channel, and some ions hit the channel walls at the Bohm velocity, and these ions are lost to the walls. The volumetric ion recombination at the walls is given as

$$S_w = n_i \bar{v}_w \sqrt{\frac{T_e}{M_{\mathrm{i}}}}, \tag{9}$$

where n_{i} is the ion density, $\bar{v}_w$ is a parameter, accounting for the radial average of the plasma density, and M_{i} is the mass of ion. As the discharge voltage increases the electron temperature increases and causes an increase in the volumetric ion production. At the same time, the ions lost to the walls also increase, due to a larger number of ions hitting the walls. As such, there is a competing nature of ion production and ion loss to the walls as the discharge voltage increases.

The propellant utilization efficiency can be expressed as

$$\eta_{\mathrm{u}} = 1-\exp\left(\frac{-L_{\mathrm{i}}(n_{\mathrm{e}}\langle\sigma_{\mathrm{i}} v_{\mathrm{e}}\rangle)}{v_{\mathrm{n}}}\right). \tag{10}$$

As mentioned by Shagayda,[55] the electron temperature at which propellant utilization has a maximum satisfies the condition

$$T_{\mathrm{e}}\frac{d\langle\sigma_{\mathrm{i}} v_{\mathrm{e}}\rangle}{d\mathrm{T_e}} - \langle\sigma_{\mathrm{i}} v_{\mathrm{e}}\rangle = 0. \tag{11}$$

When this equation is numerically solved for argon, the required electron temperature is 25.1 eV for singly charged ions, which is attained at a discharge voltage in between 250 and 300 V for TAL-type Hall thrusters operating with argon.[23] As such, the performance saturation with voltage can be attributed to both ion loss to walls and high electron temperature. Although the gain in

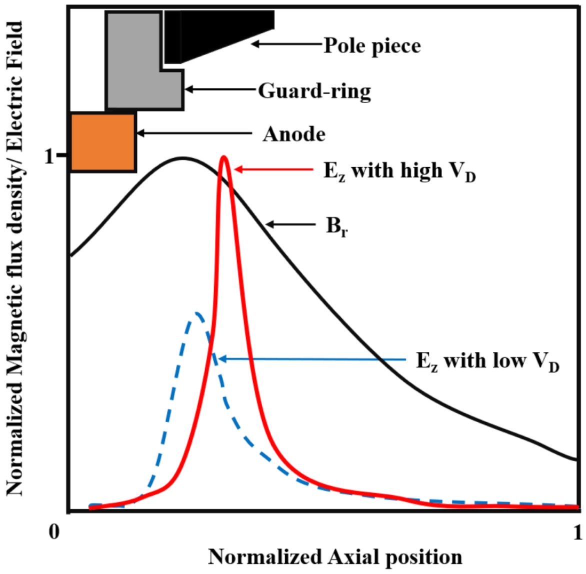

FIG. 11. Illustration of electric field distribution based on previous experiments.

propellant utilization efficiency is small when increasing voltage from 250 to 300 V, there is a greater increase in thrust when the voltage increases, regardless of the anode design choice. This is so because, in addition to the propellant utilization efficiency, thrust is influenced by beam divergence and ion velocity, which improves with increasing discharge voltage.[56,57]

The sawtooth anode enhances performance in the low-to-moderate-voltage range, but at a higher discharge voltage of 300 V, a saturation in performance gap is observed. This can be due to a difference in the exact location of the ionization based on operating conditions. Based on our previous probe experiments with RAIJIN-66 along the channel centerline,[58] the peak electric field position was found to shift by more than 1 mm when the discharge voltage increases from 200 to 300 V. An illustration of this kind of shift is shown in Fig. 11; a similar tendency has also been reported in other thrusters operating with discharge voltage up to 300 V.[59,60] As a result, in the 300 V condition, due to the ionization region being downstream of channel, the performance gap between straight and sawtooth anode is limited because neutral particles diffuse toward vacuum. In the 150 V case, the ionization region is closer to the anode and with sawtooth configuration higher neutral density aids in the performance improvement. To analytically evaluate the differences and the associated expected changes in performance, additional information on the electron density is necessary. This requires further probe experiments, and it is part of our future work.

V. CONCLUSION

This study investigated the effect of propellant flow reversal in the ionization region of RAIJIN-66, using a sawtooth hollow anode with slits cut in the anode. With an argon flow rate of 70 SCCM, the sawtooth anode successfully enhances the reflection of neutral argon atoms toward upstream and causes flow reversal, resulting in a 15.5% increase in the neutral particle density compared to a hollow anode with a straight shape of the same cross-sectional area. In the design process, the influence of angle and pitch was evaluated, and it was found that lower angles and pitch have limited improvements, and an angle of 60° was opted for manufacturing.

Straight and sawtooth anode performance evaluations were performed using different discharge voltage conditions in 50 V increments and with a fixed magnetic flux density of 45 mT. The magnetic flux density was determined by comparing the highest performance between 30, 45, and 60 mT cases, in the equilibrium anode temperature case. In the process of evaluating the appropriate magnetic flux density, importance of anode temperature control for maximum performance was also suggested. The experimental comparison between the sawtooth and straight anode at a common anode temperature of 350 K suggests a variable performance improvement depending on discharge voltage condition. When the discharge voltage is 150 V, the thrust increases by 44%, and when the discharge voltage is 250 V, the thrust increases by 5.6%.

Considering the effectiveness of the sawtooth anode, this design approach is essential in increasing the performance of Hall thrusters operating in the low efficiency regime. This includes Hall thruster operation with lighter propellants or with low discharge power. Although this study focused on TAL, a similar approach can be implemented in SPT type Hall thruster. Depending on the magnetic field design, ion losses and ionization region location can be controlled, and the effectiveness of sawtooth shaped wall can be expanded to other operating conditions than what is implemented in this study.

ACKNOWLEDGMENTS

The work was supported by the JSPS KAKENHI under Grant Nos. 24KJ0766 and 25K01416 from the Japan Society of Promotion of Science.

AUTHOR DECLARATIONS

Conflict of Interest

The authors have no conflicts to disclose.

Author Contributions

Dibyesh Satpathy: Conceptualization (lead); Data curation (equal); Formal analysis (equal); Funding acquisition (equal); Investigation (equal); Methodology (equal); Project administration (equal); Software (equal); Validation (equal); Visualization (equal); Writing – original draft (equal). **Kimiya Komurasaki:** Funding acquisition (equal); Investigation (equal); Methodology (equal); Project administration (lead); Supervision (lead); Writing – original draft (equal); Writing – review & editing (equal). **Jiwon Lee:** Data curation (equal); Formal analysis (equal); Investigation (equal); Methodology (equal); Software (equal); Validation (equal); Visualization (equal); Writing – review & editing (equal). **Hokuto Sekine:** Investigation (equal); Methodology (equal); Project administration (equal); Resources (equal); Supervision (equal); Visualization (equal); Writing – review & editing (equal). **Nadine Barth:** Data curation (equal); Formal analysis (equal); Investigation (equal); Validation (equal); Writing – review & editing (equal). **Hiroyuki Koizumi:** Methodology (equal); Resources (equal); Supervision (equal); Writing – review & editing (equal).

DATA AVAILABILITY

The data that support the findings of this study are available from the corresponding author upon reasonable request.

REFERENCES

[1]E. Y. Choueiri, "Fundamental difference between the two Hall thruster variants," Phys. Plasmas **8**, 5025–5033 (2001).
[2]L. Grimaud and S. Mazouffre, "Conducting wall Hall thrusters in magnetic shielding and standard configurations," J. Appl. Phys. **122**, 033305 (2017).
[3]D. M. Goebel, R. R. Hofer, I. G. Mikellides, I. Katz, J. E. Polk, and B. N. Dotson, "Conducting wall Hall thrusters," IEEE Trans. Plasma Sci. **43**, 118–126 (2015).
[4]M. Keidar and I. Beilis, *Plasma Engineering: Applications from Aerospace to Bio and Nanotechnology* (Academic Press, 2013).
[5]J. Simmonds, Y. Raitses, and A. Smolyakov, "A theoretical thrust density limit for Hall thrusters," J. Electr. Propuls. **2**(1), 12 (2023).
[6]L. L. Su, P. J. Roberts, T. M. Gill, W. J. Hurley, T. A. Marks, C. L. Sercel, M. G. Allen, C. B. Whittaker, E. Viges, and B. A. Jorns, "High-current density performance of a magnetically shielded Hall thruster," J. Propul. Power **40**, 729–746 (2024).
[7]I. Levchenko and K. Bazaka, "Iodine powers low-cost engines for satellites," Nature **599**, 373–374 (2021).
[8]A. Kieckhafer and L. B. King, "Energetics of propellant options for high-power Hall thrusters," J. Propul. Power **23**, 21–26 (2007).
[9]J. Szabo, B. Pote, S. Paintal, M. Robin, A. Hillier, R. D. Branam, and R. E. Huffmann, "Performance evaluation of an iodine-vapor Hall thruster," J. Propul. Power **28**, 848–857 (2012).
[10]J. M. Makela, D. R. Massey, and L. B. King, "Bismuth hollow cathode for Hall thrusters," J. Propul. Power **24**, 142–146 (2008).
[11]J. M. Makela, R. L. Washeleski, D. R. Massey, L. B. King, and M. A. Hopkins, "Development of a magnesium and zinc Hall-effect thruster," J. Propul. Power **26**, 1029–1035 (2010).
[12]K. Komurasaki and Y. Arakawa, "Hall current ion-thruster performance," J. Propul. Power **8**, 1212–1216 (1992).
[13]D. Fujita, R. Kawashima, Y. Ito, S. Akagi, J. Suzuki, T. Schönherr, H. Koizumi, and K. Komurasaki, "Operating parameters and oscillation characteristics of an anode-layer Hall thruster with argon propellant," Vacuum **110**, 159–164 (2014).
[14]D. Satpathy, H. Sekine, N. Barth, R. Kawashima, K. Komurasaki, and H. Koizumi, "Experimental investigation on ionization length required for efficient operation of argon Hall thrusters," Trans. Jpn. Soc. Aeron. Space Sci. **68**, 12–18 (2025).
[15]D. Satpathy, S. Kawabata, H. Sekine, R. Kawashima, K. Komurasaki, and H. Koizumi, "Investigation of correlation between thrust and anode temperature during transient operation of RAIJIN-66," J. Electr. Propul. **2**, 5 (2023).
[16]C. F. Book and M. L. R. Walker, "Effect of anode temperature on Hall thruster performance," J. Propul. Power **26**, 1036–1044 (2010).
[17]L. Hong, L. Xingyu, G. Zhiyong, D. Yongjie, W. Liqiu, Y. Daren, and W. Xiaogang, "Particle-in-cell simulation for effect of anode temperature on discharge characteristics of a Hall effect thruster," Plasma Sci. Technol. **20**, 125504 (2018).
[18]R. A. Martinez and M. L. R. Walker, "Propellant thermal management effect on neutral residence time in low-voltage Hall thrusters," J. Propul. Power **29**, 528–539 (2013).
[19]S. Mazouffre, G. Bourgeois, L. Garrigues, and E. Pawelec, "A comprehensive study on the atom flow in the cross-field discharge of a Hall thruster," J. Phys. D: Appl. Phys. **44**, 105203 (2011).
[20]J. Vaudolon, S. Mazouffre, C. Hénaux, D. Harribey, and A. Rossi, "Optimization of a wall-less Hall thruster," Appl. Phys. Lett. **107**, 174103 (2015).
[21]R. R. Hofer, J. B. Simmonds, D. M. Goebel, J. M. Steinkraus, and A. R. Payman, "The H10 high power density Hall thruster," J. Electr. Propul. **4**, 35 (2025).
[22]J. Miao, Q. Zhong, Q. Zhao, and X. Zhao, *Spacecraft Thermal Control Technologies* (Springer, 2021).
[23]D. Satpathy, H. Sekine, J. Lee, K. Komurasaki, R. Kawashima, and H. Koizumi, "Influence of propellant injection directionality on the performance of an argon Hall thruster," J. Appl. Phys. **136**, 233301 (2024).
[24]J. Lee, D. Satpathy, R. Kawashima, K. Komurasaki, H. Sekine, N. Barth, and H. Koizumi, "Numerical analysis of rarefied gas flow dominated by wall reflection in a straight channel," Vacuum **244**, 114930 (2025).
[25]B. M. Reid, *The Influence of Neutral Flow Rate in the Operation of Hall Thrusters* (University of Michigan, 2009).
[26]H. Fan, Y. Ding, L. Wang, Z. Chen, Y. Zhang, L. Wei, H. Li, and D. Yu, "Effects of gas supply direction on the discharge characteristics of a low-power Hall thruster," Vacuum **174**, 109193 (2020).
[27]G. Xia, H. Li, Y. Ding, L. Wei, S. Chen, and D. Yu, "Performance optimization of a krypton Hall thruster with a rotating propellant supply," Acta Astronaut. **171**, 290–299 (2020).
[28]S. Boccelli, T. E. Magin, and A. Frezzotti, "Numerical investigation of reversed gas-feed configurations for Hall thrusters," J. Propul. Power **37**, 919–927 (2021).
[29]X. Liu, H. Li, X. Che, Y. Ding, L. Wei, D. Yu, and W. Mao, "Optimizing a Hall thruster with aft-loaded magnetic field by aft-loading design of gas flow," Vacuum **222**, 112987 (2024).
[30]S. Lu, W. Luo, J. Long, F. Li, N. Guo, and L. Xu, "Numerical simulation optimization of neutral flow dynamics in low-power Hall thruster," Results Phys. **46**, 106268 (2023).
[31]F. Haotian, D. Yongjie, M. Chunjin, W. Liqiu, L. Hong, and Y. Daren, "Investigation of short-channel design on performance optimization effect of Hall thruster with large height–radius ratio," Plasma Sci. Technol. **24**, 024001 (2022).
[32]C. Xinwei, G. Jun, Y. Sanxiang, G. Hai, G. Ning, G. Zuo, Y. Juntai *et al.*, "Experimental and numerical simulation study of the effect for the anode positions on the discharge characteristics of 300 w class low power Hall thrusters," Plasma Sci. Technol. **25**, 015504 (2022).
[33]Y. Ding, H. Sun, L. Wei, P. Li, H. Su, W. Peng, and D. Yu, "A 200 W Hall thruster with hollow indented anode," Acta Astronaut. **139**, 521–527 (2017).
[34]S. Lu, C. Zhu, N. Guo, L. Dong, L. Cong, J. Wang, L. Xu, M. Wu, and J. Long, "Study of the effect of neutral flow distribution on the performance of Hall micro thruster," Vacuum **233**, 113933 (2025).
[35]Z. Xu, W. Liqiu, H. Liang, D. Yongjie, and Y. Daren, "Effect of azimuthal diversion rail on an aton-type Hall thruster," J. Phys. D: Appl. Phys. **50**, 095202 (2017).
[36]Y. Ding, H. Su, B. Jia, H. Li, L. Wei, P. Li, H. Sun, and D. Yu, "Comparative study of annular–cylindrical combined channel with annular channel Hall thruster," IEEE Trans. Plasma Sci. **46**, 4051–4059 (2018).
[37]N. Yamamoto, K. Komurasaki, and Y. Arakawa, "Discharge current oscillation in Hall thrusters," J. Propul. Power **21**, 870–876 (2005).
[38]F. Sharipov, *Rarefied Gas Dynamics: Fundamentals for Research and Practice* (John Wiley & Sons, 2015).
[39]O. V. Sazhin, S. F. Borisov, and F. Sharipov, "Accommodation coefficient of tangential momentum on atomically clean and contaminated surfaces," J. Vac. Sci. Technol. **19**, 2499–2503 (2001).
[40]Y. Hamada, J. Bak, R. Kawashima, H. Koizumi, K. Komurasaki, N. Yamamoto, Y. Egawa, I. Funaki, S. Iihara, S. Cho *et al.*, "Hall thruster development for Japanese space propulsion programs," Trans. Jpn. Soc. Aeron. Space Sci. **60**, 320–326 (2017).
[41]D. M. Goebel, I. Katz, and I. G. Mikellides, *Fundamentals of Electric Propulsion* (John Wiley & Sons, 2023).
[42]R. Kawashima, Y. Hamada, S. Kawabata, K. Komurasaki, and H. Koizumi, "Wall ion loss reduction by acceleration zone shifting in anode-layer Hall thruster," J. Propul. Power **38**, 489–493 (2022).

[43] D. L. Brown, M. L. Walker, J. Szabo, W. Huang, and J. E. Foster, "Recommended practice for use of Faraday probes in electric propulsion testing," J. Propul. Power **33**, 582–613 (2017).
[44] J. Bak, B. Van Loo, R. Kawashima, and K. Komurasaki, "Discharge characteristics and increased electron current during azimuthally nonuniform propellant supply in an anode layer Hall thruster," J. Appl. Phys. **128**, 023302 (2020).
[45] N. Nagao, S. Yokota, K. Komurasaki, and Y. Arakawa, "Development of a two-dimensional dual pendulum thrust stand for Hall thrusters," Rev. Sci. Instrum. **78**, 115108 (2007).
[46] C. White, M. K. Borg, T. J. Scanlon, S. M. Longshaw, B. John, D. R. Emerson, and J. M. Reese, "dsmcfoam+: An openfoam based direct simulation monte carlo solver," Comput. Phys. Commun. **224**, 22–43 (2018).
[47] M. O. Hedahl and R. G. Wilmoth, "Comparisons of the Maxwell and CLL gas/surface interaction models using DSMC," Technical Report, 1995.
[48] W. Huang, A. D. Gallimore, and R. R. Hofer, "Neutral flow evolution in a six-kilowatt Hall thruster," J. Propul. Power **27**, 553–563 (2011).
[49] M. Baird, T. Kerber, R. McGee-Sinclair, and K. Lemmer, "Plume divergence and discharge oscillations of an accessible low-power Hall effect thruster," Appl. Sci. **11**, 1973 (2021).
[50] I. Katz, R. R. Hofer, and D. M. Goebel, "Ion current in Hall thrusters," IEEE Trans. Plasma Sci. **36**, 2015–2024 (2008).
[51] Q. Liu, Y. Li, Y. Hu, and W. Mao, "Effects of magnetic field gradient on the performance of a magnetically shielded Hall thruster," Aerospace **10**, 942 (2023).
[52] J. Yamasaki, S. Yokota, and K. Shimamura, "Performance enhancement of an argon-based propellant in a Hall thruster," Vacuum **167**, 520–523 (2019).
[53] H. Fan, H. Li, Y. Ding, L. Wei, and D. Yu, "Effects of the peak magnetic field position on Hall thruster discharge characteristics," Adv. Space Res. **66**, 2024–2034 (2020).
[54] D. Poli, E. Bello-Benítez, P. Fajardo, and E. Ahedo, "Time-dependent axial fluid model of the Hall thruster discharge and its plume," J. Phys. D: Appl. Phys. **56**, 415203 (2023).
[55] A. A. Shagayda, "On scaling of Hall effect thrusters," IEEE Trans. Plasma Sci. **43**, 12–28 (2015).
[56] Z.-X. Ning, G.-J. Xia, X.-M. Zhu, S.-W. Chen, and D.-R. Yu, "Research on beam-focusing characteristics of krypton Hall thruster," Plasma. Phys. Rep. **45**, 537–550 (2019).
[57] D. Gawron, S. Mazouffre, N. Sadeghi, and A. Héron, "Influence of magnetic field and discharge voltage on the acceleration layer features in a Hall effect thruster," Plasma Sources Science and Technology **17**, 025001 (2008).
[58] Y. Hamada, R. Kawashima, J. Bak, K. Komurasaki, and H. Koizumi, "Characterization of acceleration zone shifting in an anode-layer-type Hall thruster RAIJIN66," Vacuum **186**, 110040 (2021).
[59] J. L. Ross, "Probe studies of a Hall thruster at low voltages," Ph.D. thesis (Michigan Technological University, 2011).
[60] K. Shirasu, H. Koizumi, H. Sekine, and K. Komurasaki, "Experimental investigation of electron-impact reactions in the plasma discharge of a water-vapor Hall thruster," J. Appl. Phys. **136**, 203302 (2024).